1   **Automated urban flood level detection based on flooded bus dataset using YOLOv8**

2   Yanbin Qiu[a], Xudong Zhou[b], Jiaquan Wan[a,*], Tao Yang[a,c], Lvfei Zhang[a], Yuanzhuo Zhong[a], Leqi Shen[a],

3   Xinwu Ji[a]

4   [a] College of Hydrology and Water Resources, Hohai University, Nanjing 210024, China

5   [b] Institute of Hydraulics and Ocean Engineering, Ningbo University, Ningbo 315000, China

6   [c] Institute of Water Resources and Technology, Hohai University, Nanjing 210024, China

7   **Corresponding Author:**

8   Jiaquan Wan

9   College of Hydrology and Water Resources, Hohai University, Nanjing 210024, China

10   Email: 775290095@qq.com

11   **ABSTRACT**

12   Rapid and accurate acquisition of urban flood information is crucial for flood prevention, disaster

13   mitigation, and emergency management. With the development of mobile internet, crowdsourced images on

14   social media have emerged as a novel and effective data source for flood information collection. However,

15   selecting appropriate targets and employing suitable methods to determine flooding level has not been well

16   investigated. You Only Look Once version 8 (YOLOv8) is a convolutional neural network-based computer

17   vision model that has been widely applied in image recognition tasks due to its end-to-end architecture and

18   high computational efficiency. This study proposes a method to assess urban flood risk levels based on the

19   submerged status of buses captured in social media images. First, a dataset containing 1008 images in

20   complex scenes is constructed from social media. The images are annotated using Labelimg, and expanded

21   with a data augmentation strategy. Four YOLOv8 configurations are validated for their ability to identify

22   urban flood risk levels. The validation process involves training the models on original datasets, augmented

23   datasets, and datasets representing complex scenes. Results demonstrate that, compared to traditional

24   reference objects (e.g., cars), buses exhibit greater stability and higher accuracy in identification of urban

25   flood risk levels due to their standardized height and widespread presence as they remain in service during

26   flood events. The data augmentation strategy enhances the model's mAP50 and mAP50-95 metrics by over

27   10% and 20%, respectively. Additionally, through comparative analysis of YOLOv8 configurations,

28   YOLOv8s demonstrates superior results and achieves an effective balance between accuracy, training time,

29   and computational resources, recommended for the identification of urban flood risk levels. This method

30   provides a reliable technical foundation for real-time flood risk assessment and emergency management of

31   urban transportation systems, with substantial potential for practical applications.

Keyword: Urban Flooding; Automatic Detection; Computer Vision; Object Detection

1. Introduction

With the intensification of global climate change, extreme precipitation events have increasingly triggered urban pluvial flooding, severely disrupting the operation of major cities (Guan et al., 2015). Concurrently, the proportion of impervious surfaces has been rising due to rapid urbanization, significantly diminishing the infiltration capacity of urban landscapes and resulting in an increase in surface runoff (Chaudhary et al., 2020). This has led to more frequent urban flooding incidents, imposing substantial impacts and losses on urban infrastructure, transportation networks, and human wellbeing. For instance, on July 20, 2021, a rare extreme rainfall event, with a record-breaking maximum hourly rainfall of 201.9 mm, driven by Typhoon In-Fa struck Zhengzhou, Henan Province, China, leading to severe urban inundation that resulted in 292 casualties and direct economic losses reaching 53.2 billion (Yang and Wang, 2022).

In the event of urban flooding, the ability to rapidly and accurately identify flood risk levels is crucial for urban flood prevention, mitigation, and emergency response decision making (Fohringer et al., 2015; Qian et al., 2022; Smith et al., 2017). Flood depth is widely regarded as the most representative indicator for assessing the severity of flood impacts. (Betterle and Salamon, 2024). The prediction of flood depth helps guide evacuation planning and resource allocation, providing decision support for emergency response and thereby significantly reducing loss of life and property damage (Jiang et al., 2020; Park et al., 2021). (Alizadeh Kharazi and Behzadan, 2021) pointed out that even 2.54 cm of floodwater can cause approximately $27,000 in combined damages to an average one-story home. When flood depth ranges between 30 to 60 cm, the risks of vehicle flotation and stalling increase substantially (Kramer et al., 2016; Pregnolato et al., 2017), posing serious threats to human safety. Moreover, flood depth information on various roads during rescue operations is essential as it influences resource allocation and rescue route planning. For example, during Hurricane Katrina, emergency responders often requested information regarding the flood extent and water depth in order to deploy appropriate vehicles for search and rescue (SAR) operations and to identify the optimal routes to reach victims (Nayak and Zlatanova, 2008). In addition, in Texas alone, it is estimated that approximately 75% of flood-related fatalities occur during evacuation efforts via local roadways, primarily due to the lack of awareness regarding inundation depth in the surrounding areas. (Alizadeh Kharazi and Behzadan, 2021). Consequently, flood depth prediction plays a vital role in assessing road passability, delineating road closures, optimizing rescue logistics, and

61   prioritizing areas for emergency intervention (Jiang et al., 2020; Kundu et al., 2022).

62   Currently, urban waterlogging monitoring primarily relies on water level gauges (Fohringer et al., 2015).

63   Although water level gauges can monitor flood depth in real-time, their deployment and maintenance are

64   costly, and the monitoring range is restricted by the installation locations, limiting their suitability for wider

65   spatial coverage (Chaudhary et al., 2020; Fohringer et al., 2015; Paul et al., 2020). Microwave remote sensing

66   methods have limitations in spatial-temporal resolution and data frequency, and are susceptible to

67   interference from clouds and obstructions, rendering them unable to determine flood depth (Chaudhary et

68   al., 2020; DeVries, 2020; Liang, 2020). An intelligent and low-cost technology capable of identifying urban

69   flood risks with extensive spatial coverage is urgently needed.

70   In recent years, with the rapid development of social media and mobile internet, the application of social

71   media data in flood monitoring and risk assessment has garnered extensive attention (Baranowski et al., 2020;

72   Kankanamge et al., 2020; Li et al., 2023; Rosser et al., 2017; Smith et al., 2017). Platforms like Weibo,

73   Twitter and Douyin provide users with channels to share flood information in real time, where user-generated

74   content (UGC) contains rich flood imagery and geolocation data, offering a novel data source for urban flood

75   level detection research (Iqbal et al., 2021). Concurrently, significant advancements have been made in

76   computer vision technology, particularly in the application of convolutional neural networks (Voulodimos

77   et al., 2018) , opening new avenues for the analysis of vast amounts of flood imagery data. Current studies

78   have attempted to use objects in social media images, such as bridges (Bhola et al., 2018), roadside barriers

79   (Jiang et al., 2019), bicycles (Chaudhary et al., 2020), traffic cones (Jiang et al., 2020), traffic signs (Alizadeh

80   Kharazi and Behzadan, 2021), water level markers (Jafari et al., 2021), and pedestrians (Li et al., 2023), as

81   reference points for flood level estimation. While specific reference objects have shown promising results

82   in studies, their infrequent occurrence hinders their broad application in urban settings. Pedestrians are

83   prevalent in urban areas, but their low image resolution and diminished presence in severely flooded zones

84   reduce their reliability and practicality as reference points for water level estimation.

85   Vehicles serve as ideal reference objects for recognizing urban flood levels, attributed to their stable

86   morphological features, widespread availability, and ease of detection. Current research leverages vehicles

87   for urban flood water level identification. For example, (Park et al., 2021) and (Huang et al., 2020) used

88   Mask R-CNN to detect the submerged state of vehicles or their wheels as an indicator of flood levels. Wan

89   et al. utilized the YOLO (You Only Look Once) series models, a CNN-based computer vision (CV) model,

90 for urban flood risk assessment and detection (Puliti and Astrup, 2022; Redmon et al., 2016; Wan et al.,

91 2024; Zhong et al., 2024). However, most studies use cars as reference objects; yet, the diversity of car types

92 (e.g., sedans, SUVs, and pickup trucks) introduces significant variations in height and dimensions, affecting

93 model generalization. Furthermore, the limited height of car bodies means they cannot provide effective

94 water level information once submerged up to the roof, and their lower frequency of appearance in extreme

95 weather makes it challenging to collect image datasets.

96   In comparison, buses, as a critical component of urban transportation systems, possess standardized

97 heights and structures with minimal variation between models, making them a more ideal reference object

98 for flood water level monitoring. Buses overcome the limitations posed by cars, such as variations in size

99 and limited height. Additionally, buses primarily operate in busy or essential areas, and their ability to

100 withstand submersion is crucial for the continued operation of the urban public transportation system. Flood

101 level recognition based on the submerged status of buses can intelligently assess their water-related risks,

102 providing valuable support for urban transportation emergency management.

103   In response to the gaps in existing research, this study aims to create a comprehensive dataset of

104 submerged buses by sourcing flood images from social media platforms. Based on urban flood safety

105 standards and bus height characteristics, the submerged states of buses are categorized into specific levels.

106 The dataset includes complex scenes (e.g., nighttime, occlusions, and incomplete bus bodies) to enhance

107 data diversity.

108   YOLO is an efficient real-time object detection algorithm that simplifies the traditional multi-stage

109 detection pipeline by framing object detection as a regression problem. In the YOLO model, the image is

110 divided into a grid, with each grid cell predicting the location (bounding box) and class probability of an

111 object. The uniqueness of YOLO lies in its ability to predict multiple bounding boxes simultaneously in a

112 single forward pass, significantly improving computational efficiency and processing speed. The model

113 utilizes a convolutional neural network for feature extraction and considers the global context of the image,

114 which helps reduce the likelihood of false positives. The YOLOv8 algorithm, as the most recent iteration of

115 the YOLO series, has exhibited outstanding accuracy and rapid detection performance on the standard

116 COCO (Common Objects in Context) dataset (Wan et al., 2024). In this study, the YOLOv8 model is trained

117 on the purpose-built dataset to improve its performance in identifying urban flood water levels with precision.

118   This study introduces an innovative approach to flood level detection by leveraging the submerged

119   states of buses, addressing the limitations of traditional recognition methods based on cars and other

120   reference objects and overcoming the limitations of conventional monitoring techniques in broader

121   applications. Specifically, the objectives of this study include:

122   1)   Developing a comprehensive dataset of submerged buses to examine the relationship between bus

123   submersion and flood water levels.

124   2)   Evaluating the performance of YOLOv8 configurations in assessing flood severity through original and

125   augmented data training, as well as experiments involving complex scenes.

126   3)   Proposing configuration recommendations for YOLOv8 aims to address diverse application scenarios,

127   ensuring efficient deployment in varied urban environments.

128   This paper is structured as follows: Section 2 provides a detailed description of the dataset construction,

129   data augmentation strategies, YOLOv8 model configurations and explains the experimental design and

130   model evaluation metrics. Section 3 explains experimental results, followed by a comparative analysis of the

131   findings. Section 4 discusses the experimental results and offers configuration recommendations for

132   YOLOv8. Finally, Section 5 provides a summary of the main conclusions and highlights potential directions

133   for future research.

134   **2. Methodology**

135   **2.1 Data acquisition and processing**

136   **2.1.1 Data acquisition**
137   In this study, a comprehensive dataset of submerged buses was constructed, comprising 1,008 images

138   that capture buses in various statues of submersion. These submerged bus images were collected through

139   keyword searches such as urban flooding and submerged bus on Baidu and Google, screenshots of relevant

140   frames in short videos on Douyin, browsing urban flood news, and obtaining images from WeChat public

141   accounts. Due to the diverse sources of image data, the images used in the experiment vary in resolution and

142   size. When selecting bus images, this study included complex and challenging scenes, such as nighttime

143   scenes, partial occlusions, and incomplete buses, to ensure the dataset's diversity. The inclusion of these

144   scenes may help enhance the diversity of the dataset, potentially enabling the trained model to better handle

145   various flood scenes.

146   All collected images of buses were manually screened to ensure that the depicted buses were either

147   stationary or normally moving through floodwater during flooding events, without signs of floating or water-

148   induced displacement. This process ensured the validity and reliability of buses as stable reference objects.

149   **2.1.2 Data annotation**

150   This study assesses flood risk levels based on the submersion status of buses. In this study, the

151   approximate height of buses was uniformly set to 3 meters in the model, based on the specifications of

152   commonly observed urban bus types in social media images. Based on a systematic evaluation of the images,

153   it was found that the submersion depths of buses were mostly concentrated between 0 and 50 cm, with values

154   exceeding 100 cm observed only in a few cases. Given that high water levels (greater than 100 cm) are

155   relatively rare in urban scenarios, this study chooses to define classification levels within the more commonly

156   observed water depth range. Consequently, four flood levels were established, with detailed information on

157   each flood level and corresponding bus examples provided in Table 1. Using Labelimg, a widely used

158   annotation tool for object detection model training, the 1,008 acquired images were annotated to identify

159   1,562 bus instances, which were stored in YOLO format for subsequent training. Based on different states

160   of bus movement, annotation types were divided into two categories: holistic and segmented. In holistic

161   annotation, the entire bus is assigned a single flood level, while in segmented annotation, specific parts of

162   the bus correspond to different levels, as illustrated in Fig. 1.

163   **Table 1**

164   Flooded bus dataset: bus instances and flood levels.

Flood levels	Analysis of bus submersion depths	Range of water depth	Number of instances
Level1	bottom of wheels submerged; inner wheel contour not visible	0~20 cm	296
Level2	between bottom of wheels and halfway up the tires, between bottom of wheels and top edge of license plate, water reaches 1/4 of the step at bottom of door	20~45 cm	585
Level3	between halfway up the tires and full tire coverage, between top edge of license plate and bottom edge of windshield	45~100 cm	371
Level4	above the bottom edge of the windshield, fully submerged tires	>100 cm	310

165

(a) The entire bus is assigned a single flood level

(b) The specific part of bus is assigned different levels

Fig. 1. Examples of dataset annotations: (a) The entire bus is assigned a single flood level; (b) The specific part of bus is assigned different levels.

2.1.3 Data augmentation

The original dataset, comprising 1,008 images, is relatively small in scale, necessitating its enhancement and expansion to increase background complexity, prevent overfitting, and improve robustness. Image data augmentation methods can be broadly categorized into two types: luminosity distortions and geometric distortions(Li et al., 2023). The former involves adjusting image brightness, contrast, hue, saturation, and adding noise, while the latter encompasses random scaling, cropping, flipping, and rotation operations. In this study, horizontal and vertical flipping, rotation, and random cropping were applied to augment the original dataset, as illustrated in Fig. 2. All images in the augmented dataset were annotated using Labelimg and stored in YOLO format. Additionally, considering the potential for manual annotation bias, a review process was conducted to verify the correctness of all bounding boxes and annotations related to flood risk levels.
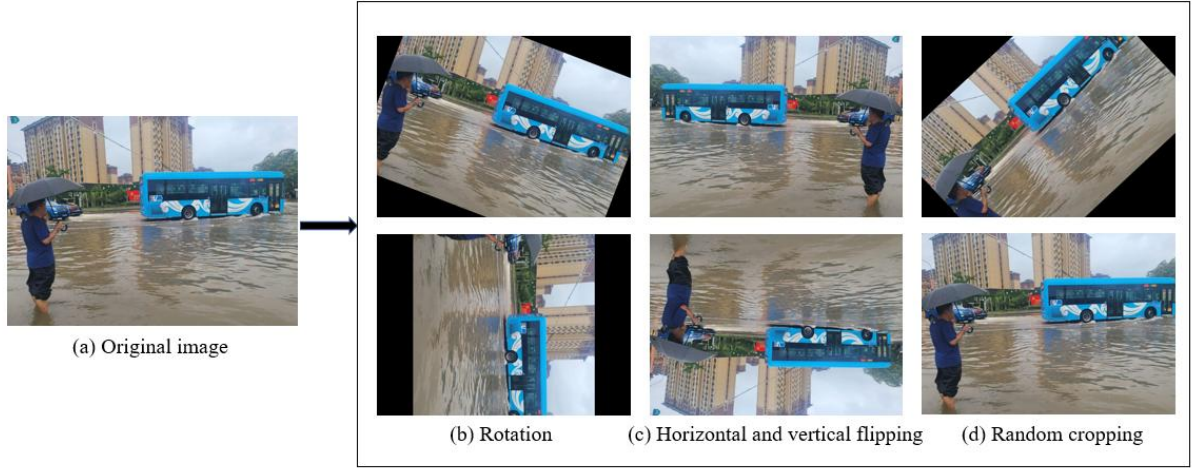
Fig. 2. Examples of dataset augmentations: (a) Original image; (b) Rotation; (c) Horizontal and vertical flipping; (d) Random cropping.

2.2 Object detection model

A key feature of the YOLO model is its ability to achieve an optimal trade-off between speed and accuracy, enabling rapid and precise object detection across a wide range of application scenes (Wan et al., 2024). This study constructed an object detection model based on the YOLOv8 source code, which operates on convolutional neural networks (CNN). YOLOv8 is an integrative and enhanced version building on previous YOLO generations and represents the latest iteration in the YOLO series. This version significantly improves computational efficiency and inference speed by optimizing the network architecture and refining inference algorithms. Moreover, YOLOv8 demonstrates higher stability in multi-object detection tasks under complex scenes, particularly with its advanced features such as automated hyperparameter tuning and dynamic convolution modules. These enhancements further boost the model's flexibility and adaptability, making it more capable of meeting the diverse requirements of real-world applications.

The YOLOv8 processing workflow includes image preprocessing, multi-level feature extraction through CNN, and multi-scale feature fusion via a feature pyramid and path aggregation network. Following this, adaptive anchor boxes are used for bounding box regression and classification prediction, with non-maximum suppression applied to eliminate redundant bounding boxes. The model ultimately outputs the target's class, bounding box, and confidence score, ensuring a balance between detection accuracy and efficiency.

As shown in Fig. 3, the YOLOv8 network architecture is composed of three primary parts: Backbone, Neck, and Head. The Backbone consists of five convolutional modules, four C2f modules, and a Spatial Pyramid Pooling-Fast (SPPF) module, all designed for feature extraction. The Neck refines and integrates

203 features derived from the Backbone, improving both the precision and reliability of object detection. The

204 Head utilizes a decoupled structure to handle feature maps across multiple scales, generating the final

205 detection outputs.
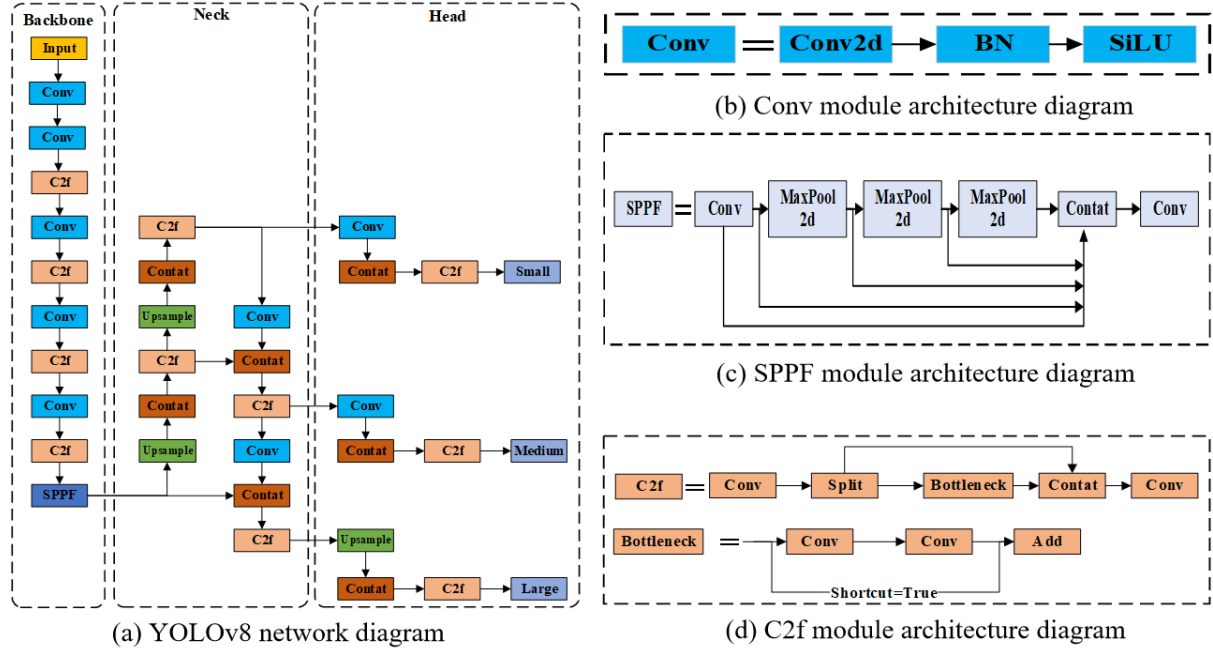
206
207 **Fig. 3.** The YOLOv8 network structure: (a) YOLOv8 network diagram; (b) Conv module architecture
208 diagram; (c) SPPF module architecture diagram; (d) C2f module architecture diagram.

209 **2.2.1 Experiment on object detection model**
210 Following data augmentation, the original dataset was expanded to 2,184 images for model training. In

211 this study, four different YOLOv8 configurations—YOLOv8n, YOLOv8s, YOLOv8m, and YOLOv8l—

212 were used for training, each designed with specific network depths and widths to address varying application

213 requirements. Table 2 presents the key characteristics of these four YOLOv8 configurations. The number of

214 layers reflects the depth of the model, with a greater number of layers indicating a deeper model capable of

215 capturing higher-level semantic features. However, this also leads to increased computational complexity.

216 Parameters refer to the total number of learnable weights and biases within the model. A higher number of

217 parameters signifies stronger representational capacity, making the model suitable for more complex tasks,

218 but it also requires greater computational resources and longer training times.

219 **Table 2**
220 The primary characteristics of the four YOLOv8 configurations.

Model	Size	Layers	Params (M)	mAP50-95on val (%)	FLOPs (B)	Speed CPU ONNX (ms)	Speed A100 TensorRT (ms)
YOLOv8n	640	225	3.2	37.3	8.7	80.4	0.99
YOLOv8s	640	225	11.2	44.9	28.6	128.4	1.20
YOLOv8m	640	295	25.9	50.2	78.9	234.7	1.83
YOLOv8l	640	365	43.7	52.9	165.2	375.2	2.39

2.2.2 Experimental setup

The model was implemented using PyTorch, a framework offering libraries for object detection models. Training was performed on NVIDIA Quadro RTX 3090 GPU. The original dataset contained 1,008 images, with 90% allocated for training and the remaining 10% for validation. The initial input size was set to 640×640, with a batch size of 16 and 100 training epochs. In the data augmentation experiment, augmentation was applied only to the training set, resulting in 1,986 augmented training images. To maintain a consistent 90%-10% split ratio, the validation set was expanded from 108 to 198 images using non-augmented and previously unused images, while all other settings remained the same as previously described. Throughout the entire training process, the validation set was strictly separated from the training set, and the model had no access to any original or augmented images from the validation set. In this study, the official default hyperparameter settings of YOLOv8 were adopted.

2.2.3 Complex scenes prediction experiment

The performance of object detection models on the validation dataset does not fully represent its overall capabilities, as view of the bus, impacted by camera angle and distance, introduces numerous sources of interference. To address this, a complex scene prediction experiment was designed in this study to assess the detection capabilities of the different YOLOv8 configurations under challenging urban flood environments.

In this experiment, YOLOv8 models trained on either the original or augmented datasets were used to conduct complex scene predictions, evaluating their performance under challenging conditions. Fig. 4 presents two particularly demanding scenes, not in the existing dataset, Fig. 4a shows a rainy scene with multiple vehicles, where the incomplete view of the bus, impacted by camera angle and distance, introduces numerous sources of interference, increasing detection complexity. Fig. 4b depicts a nighttime scene of a submerged bus, where low light and poor image quality significantly elevate the difficulty of detection.
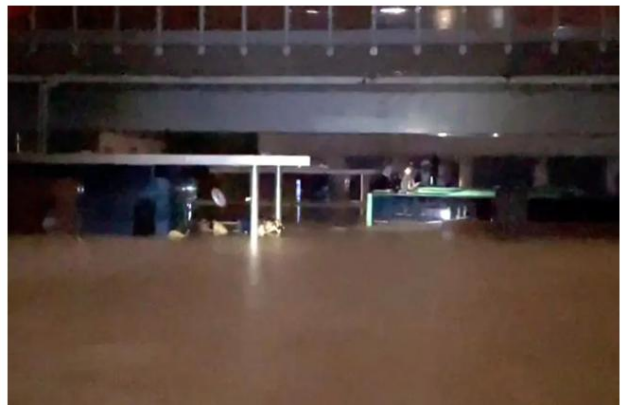
(a) Low flood risk scene with multiple vehicles present   (b) High flood risk scene with blurring and corruption

244 **Fig. 4.** Two complex urban flooding scenes: (a) Low flood risk scene with multiple vehicles present; (b)
245 High flood risk scene with blurring and corruption.

2.2.4 Comparative experiment with YOLOv5 model

247   Although the introduction states that YOLOv8 is the latest algorithm in the YOLO series, the absence

248 of comparative experimental results with earlier YOLO versions weakens the argument for its superior

249 performance. This study will compare and analyze the configuration demonstrating superior performance in

250 the experiments with the corresponding configuration in the YOLOv5 model. The experiments include

251 training on the original dataset, training with data augmentation, and complex scene prediction, following

252 the same experimental setup described earlier.

2.3 Model evaluation

254   The widely recognized evaluation metrics, such as precision (P), recall (R), and F1 scores are as follows:

$$Precision = \frac{TP}{TP + FP} \tag{1}$$

$$Recall = \frac{TP}{TP + FN} \tag{2}$$

$$F1 = \frac{2 \times Precision \times Recall}{Precision + Recall} \tag{3}$$

258   Precision (P) quantifies the model's false detection rate, while Recall (R) evaluates its true detection

259 rate. The F1-score evaluates model performance, particularly in object detection tasks, as it combines both

260 P and R, representing their harmonic mean, where True Positive (TP) refers to the count of objects correctly

261 identified as positive, True Negative (TN) denotes the count of non-objects accurately classified as negative,

262 False Positive (FP) indicates the count of non-objects incorrectly classified as positive, and False Negative

263 (FN) represents the count of objects wrongly classified as negative.

264   In this study, mean Average Precision (mAP), a well-established evaluation indicator, is utilized as the

265 primary criterion to evaluate the performance of different YOLOv8 configurations in detecting bus

266 submersion states. The mAP is computed by summing the average precision across all labels and dividing

267 the result by the total number of categories. A higher mAP value signifies improved average accuracy of the

268 model, indicating enhanced overall detection performance. The formula for calculating mAP is as follows:

$$mAP = \frac{1}{n}\sum_{i=1}^{n} AP_i = \frac{1}{n}\sum_{i=1}^{n} \int_0^1 P_i(R_i)dR_i \tag{4}$$

270   where n is the number of categories, Average Precision (AP) is the area under the Precision–Recall (P–

271 R) curve, P is used to measure the false detection rate of the model and R is used to measure the true detection

272 rate, the formulas for P and R are given in Equations (1) and (2).

273   Intersection over union (IoU) is a fundamental metric in object detection that measures the degree of

274 overlap between the predicted bounding box (generated by the algorithm) and the ground truth bounding

275 box (annotated using labeling software), with a range of values from 0 to 1. A higher IoU value signifies

276 better prediction accuracy, representing a greater overlap between the predicted bounding box and the ground

277 truth bounding box. The formula for calculating IoU is as follows:

278
$$IoU = \frac{A \cap B}{A \cup B}$$
(5)

279   where A denotes the area of the detection box, while B refers to the area of the ground truth box.

280   IoU is widely used to determine whether a predicted bounding box is considered a true positive. As the

281 output quality of the model varies with changes in the Intersection over Union (IoU) threshold, it is standard

282 practice to evaluate model performance across multiple IoU thresholds.

283   mAP50 and mAP50-95 are core metrics for evaluating object detection model performance, each

284 measuring the model's average detection precision under different IoU threshold conditions. mAP50

285 indicates the average precision computed at an IoU threshold of 0.5, where an overlap of over 50% between

286 the detection box and ground truth box qualifies as a correct detection. This metric primarily reflects the

287 model's basic object detection capability. mAP50-95, on the other hand, is the mean average precision

288 calculated across ten different IoU thresholds, from 0.5 to 0.95 in 0.05 increments. This metric averages AP

289 across multiple IoU thresholds, providing a comprehensive assessment of the model's performance. A higher

290 mAP50-95 value indicates stronger generalization ability across varying degrees of overlap within the same

291 scene. Collectively, mAP50 and mAP50-95 provide a thorough and objective evaluation of model prediction

292 accuracy and are extensively utilized in the domain of object detection.

293 **3. Result**

294 **3.1 Training experimental results**

295 **3.1.1 Analysis of training results on the original dataset**
296   This subsection provides a comparative evaluation of the training outcomes of the different YOLOv8

297 models on the original dataset. Each model was trained under the experimental settings outlined in Section

298 3.1. Fig. 5 illustrates the trend of mAP for each model during the training period, while Fig. 6 presents the

299   prediction performance of each model across individual classes.

300   As illustrated in Fig. 5a, following 100 epochs of training, the four models (YOLOv8n, YOLOv8s,

301   YOLOv8m, YOLOv8l) each reach convergence, achieving mAP50 values on the validation dataset of 0.618,

302   0.662, 0.611, and 0.639, respectively. YOLOv8s exhibits superior performance in this object detection task,

303   maintaining a higher mAP50 across the training duration compared to the other configurations. YOLOv8l

304   shows pronounced oscillations during the early training stages, requiring a longer stabilization period.

305   Furthermore, it is observable that mAP50 for all models increases rapidly in the early epochs (0-20), after

306   which the growth rate decelerates and plateaus. Notably, an increase in network width (param) and depth

307   (layer) for YOLOv8 does not yield a substantial improvement in mAP50.

(a) The trend of mAP50   (b) The trend of mAP50-95
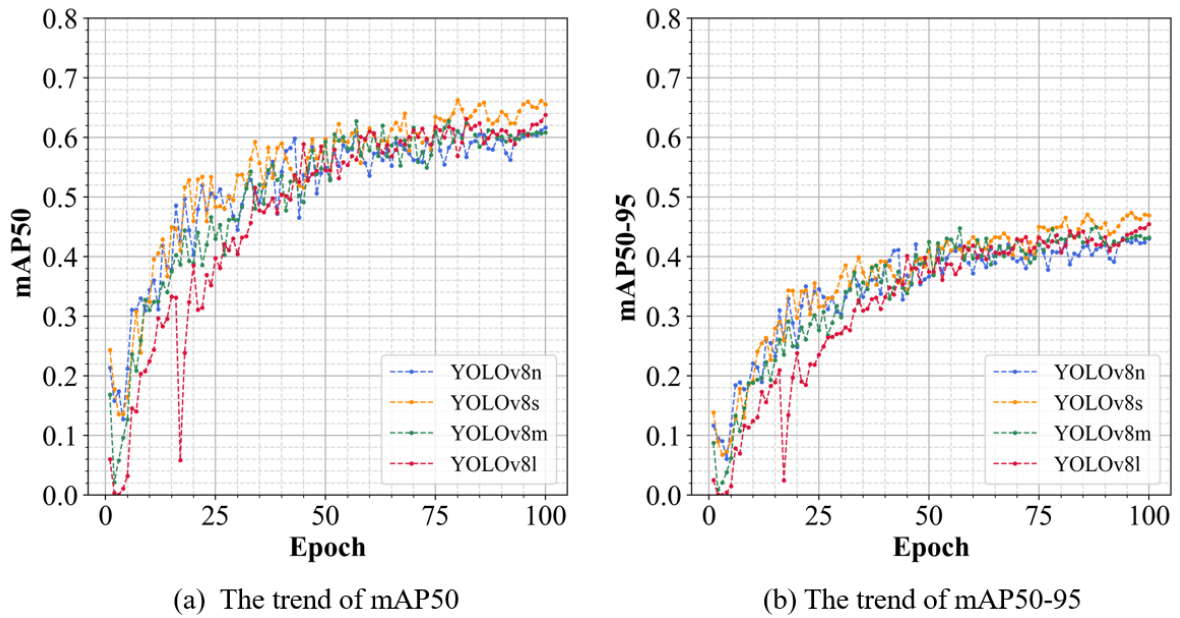
308
309   **Fig. 5.** The mAP of the validation dataset throughout the training process (a) The trend of mAP50; (b) The

310   trend of mAP50-95.

311   As shown in Fig. 6, the detection performance of the four YOLOv8 models varies across different flood

312   risk levels. The YOLOv8s model demonstrates superior average precision across all flood risk categories,

313   with an mAP50 of 0.662. For low flood risk category identification (level 1), all models achieve satisfactory

314   detection results. However, for higher flood risk categories, the detection performance of YOLOv8n,

315   YOLOv8m, and YOLOv8l is below expectations, with only YOLOv8s effectively capturing the submersion

316   characteristics of buses at high water levels, thereby achieving relatively accurate identification. Although

317   the YOLOv8l model has higher complexity and a larger parameter scale, its AP values for the level 3 and

318   level 4 categories are 0.591 and 0.530, respectively, significantly lower than those of the YOLOv8s model,

319   which are 0.632 and 0.602. This suggests that, for detecting high flood risk features, increased model

320   complexity does not inherently result in improved detection accuracy.
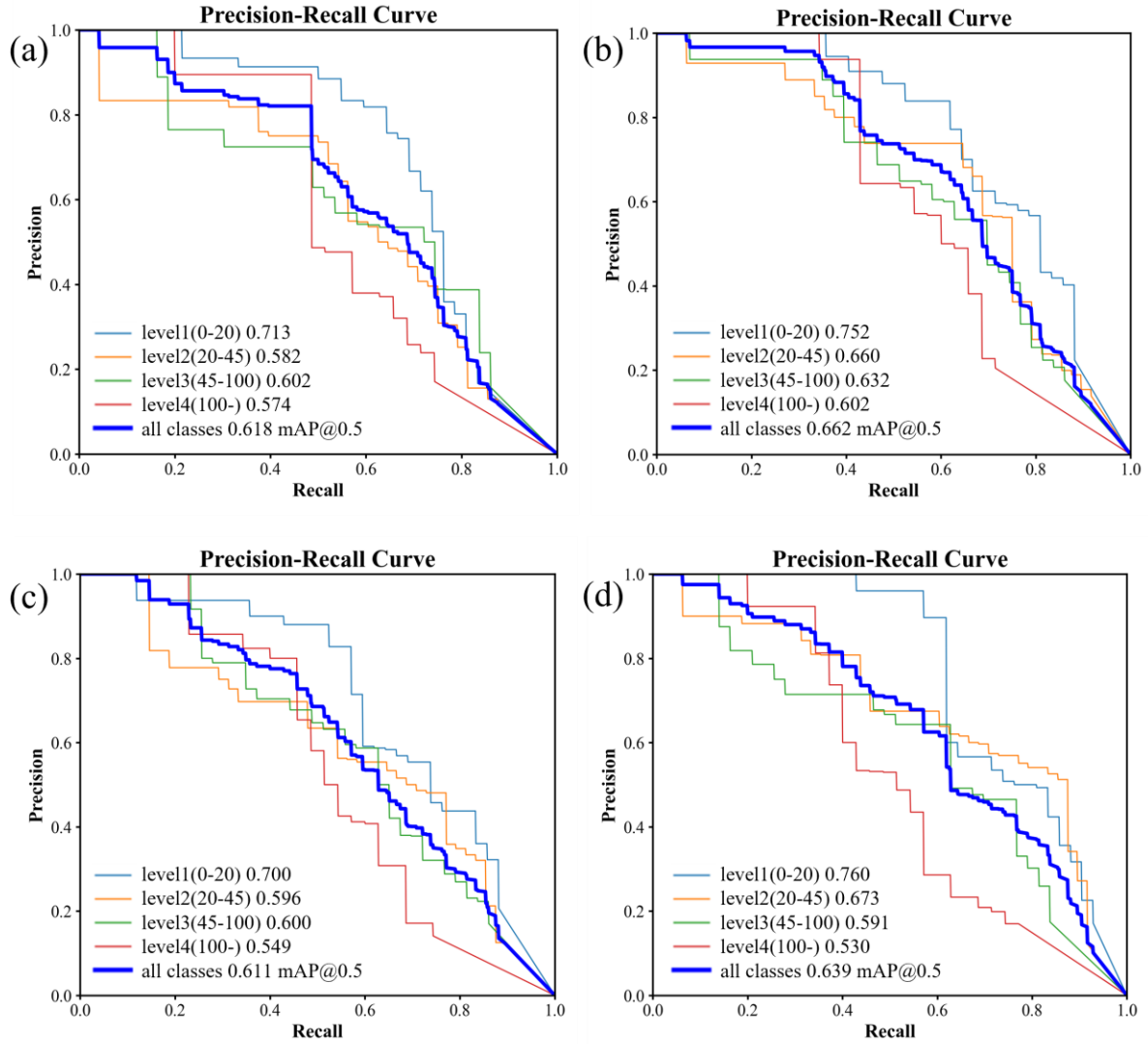
321
322   **Fig. 6.** Precision-recall curve for each class of validation process: (a) YOLOv8n Validation Results; (b)
323   YOLOv8s Validation Results; (c) YOLOv8m Validation Results; (d) YOLOv8l Validation Results.

324   **3.1.2 Analysis of training results on the augmented dataset**
325   This subsection compares the training performance of different YOLOv8 models on the augmented

326   dataset. Fig. 7 illustrates the mAP trend, while Fig. 8 presents the prediction performance of each model.

327   As depicted in Fig. 7a, after 100 training epochs, the four models (YOLOv8n, YOLOv8s, YOLOv8m,

328   YOLOv8l) all converge, reaching mAP50 values on the validation dataset of 0.722, 0.734, 0.716, and 0.703,

329   respectively. Among them, YOLOv8s consistently outperforms the other models. The early-stage

330   fluctuations observed during YOLOv8l training disappear, resulting in smoother curves and a more stable

331   optimization process. However, compared to other models, the performance improvement of YOLOv8l

332   during the early stages of training remains relatively slower. This may be attributed to the model's higher

333   complexity and larger parameter scale.

(a) The trend of mAP50   (b) The trend of mAP50-95
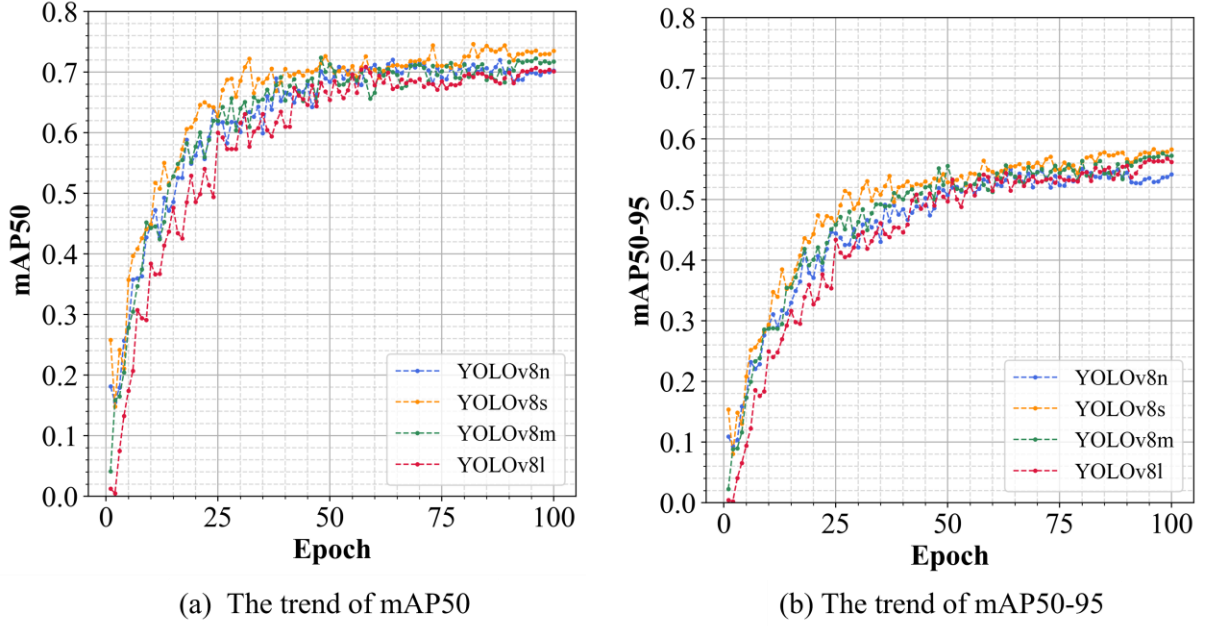
334
335 **Fig. 7.** The mAP of the validation dataset throughout the training process after data augmentation: (a) The
336 trend of mAP50; (b) The trend of mAP50-95.

337   As illustrated in Fig. 8, following data augmentation, the four YOLOv8 models exhibit similar

338 performance in detecting each flood risk level. The highest overall effectiveness is found in YOLOv8s,

339 achieving an mAP50 of 0.734, with consistently high precision and recall across all flood risk categories.

340 All models effectively capture the submergence characteristics of buses at various water levels, with AP

341 values for each category exceeding 0.67, indicating robust performance on the validation dataset.

342   Notably, the detection results for higher-risk categories (Level 3 and Level 4) show improved AP values

343 in all models, as evidenced by the Precision-Recall curves shifting closer to the upper-right corner. For

344 example, in the YOLOv8n model, the AP value for Level 3 increased from 0.602 to 0.712, and for Level 4,

345 from 0.574 to 0.746. Similarly, in the YOLOv8l model, the AP value for Level 3 rose from 0.600 to 0.685,

346 and for Level 4, from 0.549 to 0.679. This improvement is primarily attributed to enhanced data diversity,

347 effectively mitigating the interference caused by variations in viewpoint and object scale. This not only

348 improved the model's ability to detect higher-level targets but also enhanced the overall detection

349 performance.
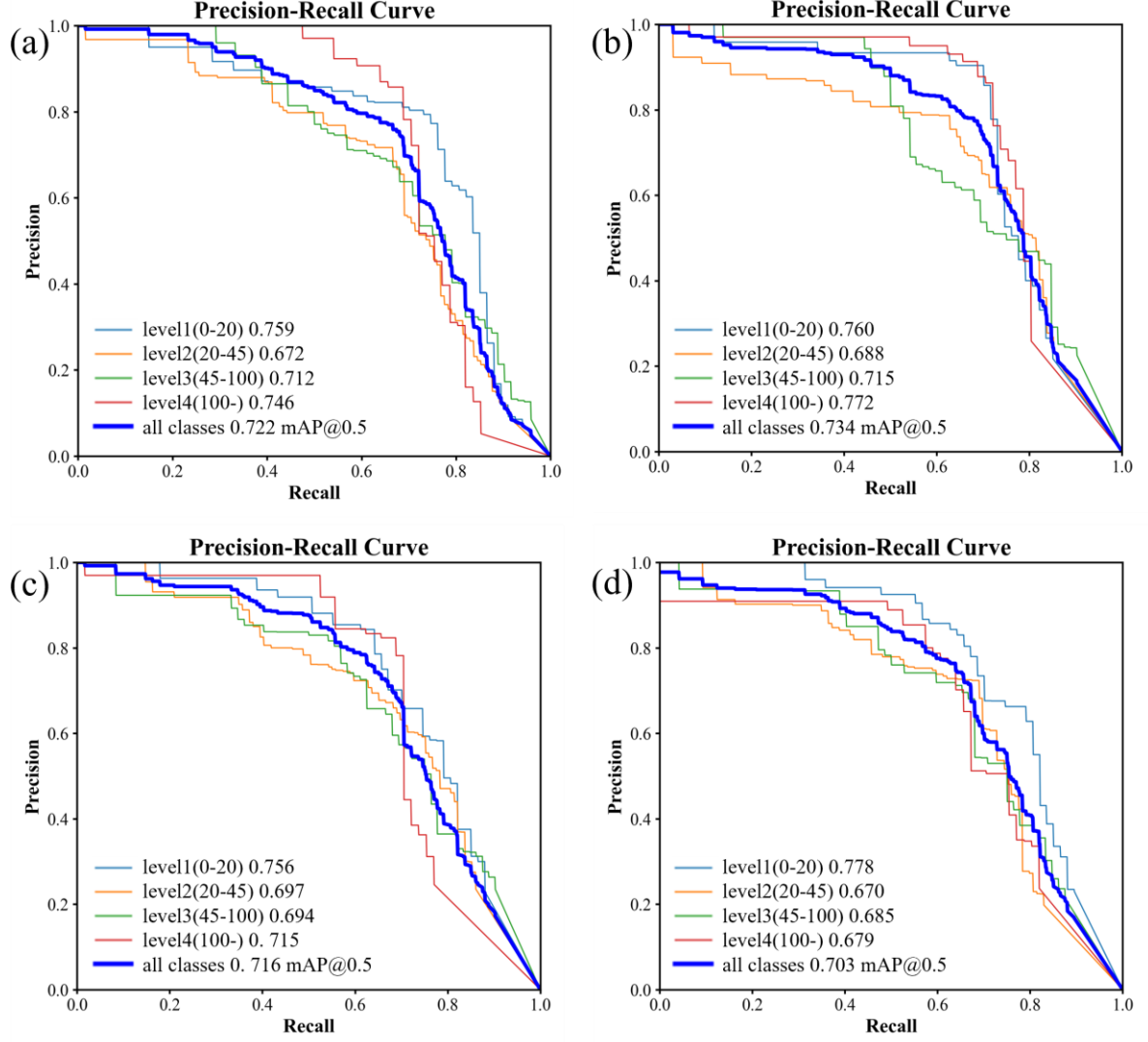
Fig. 8. Precision-recall curve for each class of validation process after data augmentation: (a) YOLOv8n Validation Results; (b) YOLOv8s Validation Results; (c) YOLOv8m Validation Results; (d) YOLOv8l Validation Results.

This study provides a comparative analysis of the detection performance of different YOLOv8 model configurations before and after data augmentation. Table 3 presents the mAP50, mAP50-95, and training times for the optimal YOLOv8 models

Table 3

mAP and training time for four YOLOv8 configurations: pre- and post-data augmentation.

YOLO v8	mAP50 (%)			mAP50-95 (%)			training time (h)	
	original dataset	augmented dataset	incre ase	original dataset	augmente d dataset	incre ase	original dataset	augmented dataset
n	61.7	72.2	17.0	43.0	55.2	28.4	0.102	0.325
s	66.0	73.4	11.2	47.5	58.2	22.5	0.152	0.483
m	61.2	71.6	17.0	45.0	57.4	27.6	0.293	0.930
l	63.8	70.3	12.2	45.4	56.6	24.7	0.438	1.390

As indicated in Table 3, improvements in detection performance were observed across all model configurations when trained on the augmented dataset. For mAP50, all models demonstrated improvements exceeding 10%, while mAP50-95 gains surpassed 20% for each configuration. YOLOv8m and YOLOv8n

exhibited the highest mAP50 increases, whereas YOLOv8s showed the smallest gain at 11.2%. In terms of mAP50-95, YOLOv8n achieved the greatest improvement, rising from 43.0% to 55.2% (28.4% increase), while YOLOv8s displayed the smallest increase at 22.5%.

In terms of overall performance, YOLOv8s achieved the highest mAP50 and mAP50-95 values across all configurations, reaching 73.4% and 58.2%, respectively, with a moderate training time. By contrast, YOLOv8l achieved similar mAP50 and mAP50-95 values but required nearly triple the training time. Similarly, YOLOv8m showed performance close to that of YOLOv8s, though with a nearly doubled training time.

3.2 Experimental results in complex scenes

3.2.1 Validation results of models on the original dataset

This section presents a comparative evaluation of the validation outcomes for the four optimized YOLOv8 models trained on the original dataset. The numbers in the top-right corner of the detection boxes (ranging from 0 to 1) represent the confidence level of the model for the detection results. As shown in Fig. 9, all four models can detect the flood risk level of the bus. However, only YOLOv8l correctly identifies it as level 1, albeit with low confidence, while the other models incorrectly classify it as level 2. At low flood risk levels, none of the models effectively capture the critical distinguishing features, highlighting limitations in their generalization capabilities.

(a) Detection outcomes obtained using YOLOv8n (b) Detection outcomes obtained using YOLOv8s

(c) Detection outcomes obtained using YOLOv8m (d) Detection outcomes obtained using YOLOv8l

Fig. 9. Comparison of YOLOv8 detection results in low flood risk scene with multiple vehicles present (pre-augmentation): (a) Detection outcomes obtained using YOLOv8n; (b) Detection outcomes obtained using YOLOv8s; (c) Detection outcomes obtained using YOLOv8m; (d) Detection outcomes obtained using YOLOv8l.

Moreover, Fig. 10 presents the validation results at a high flood risk level. All four optimal YOLOv8 models successfully detect the blurred bus in the image and identify its submerged state with high confidence. For the bus located at the upper-right edge of the image, none of the models detected it due to low lighting, though they were able to make partial level assessments. The models have learned to extract key features associated with incomplete bus bodies from the dataset. Furthermore, YOLOv8l incorrectly classified the bus station and surrounding environment as level 4 submersion.

(a) Detection outcomes obtained using YOLOv8n

(c) Detection outcomes obtained using YOLOv8m
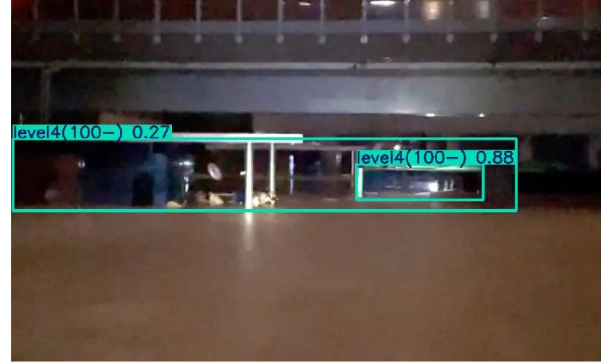
(d) Detection outcomes obtained using YOLOv8l

Fig. 10. Comparison of YOLOv8 detection results in high flood risk scene with blurring and corruption (pre-augmentation): (a) Detection outcomes obtained using YOLOv8n; (b) Detection outcomes obtained using YOLOv8s; (c) Detection outcomes obtained using YOLOv8m; (d) Detection outcomes obtained using YOLOv8l.

3.2.2 Validation results of models on the augmented dataset

This section provides a comparative evaluation of the validation outcomes for the four optimized YOLOv8 models after data augmentation. As shown in Fig. 11, all four models accurately detect the flood risk level of the bus with high confidence. In this detection, the best performance is found inYOLOv8n, exhibiting higher confidence levels than the other models. Besides, both YOLOv8s and YOLOv8m unexpectedly generated a level 2 prediction box during bus detection.
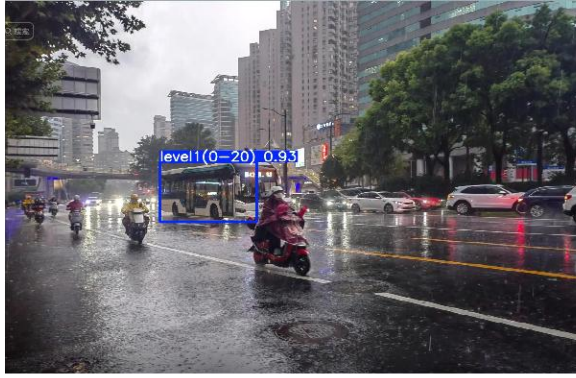
(a) Detection outcomes obtained using YOLOv8n   (b) Detection outcomes obtained using YOLOv8s
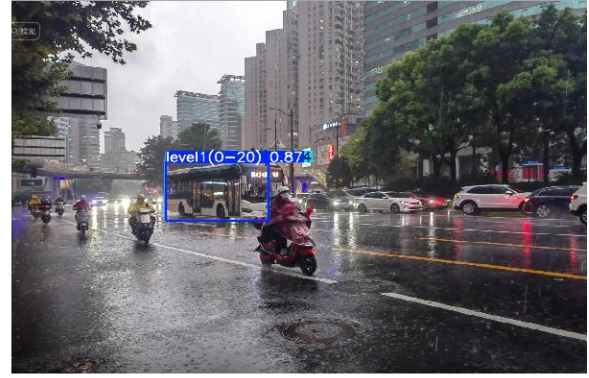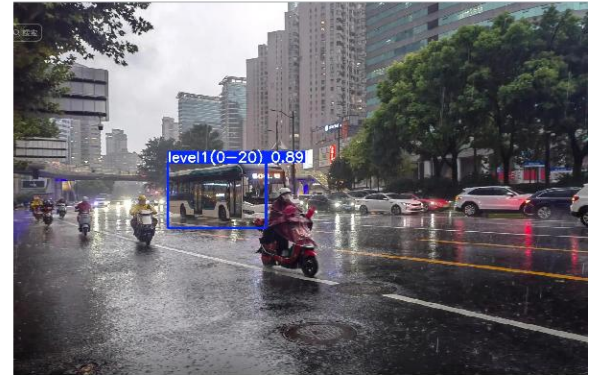
(c) Detection outcomes obtained using YOLOv8m   (d) Detection outcomes obtained using YOLOv8l

Fig. 11. Comparison of YOLOv8 detection results in low flood risk scene with multiple vehicles present (post-augmentation): (a) Detection outcomes obtained using YOLOv8n; (b) Detection outcomes obtained using YOLOv8s; (c) Detection outcomes obtained using YOLOv8m; (d) Detection outcomes obtained using YOLOv8l.

Fig. 12 presents the validation results at a high flood risk level. All four optimal YOLOv8 models successfully detect the blurred bus in the image, accurately identifying its submerged state with high confidence. The highest confidence is found in YOLOv8s, without any false detections. However, none of the models detected the bus body located at the upper-right edge of the image, even after data augmentation. Besides, YOLOv8m and YOLOv8l incorrectly classified the bus station and background environment as level 4 submersion.

In summary, improvements in recognition accuracy and confidence were observed across the four optimal models when trained with augmented data, supporting more reliable detection of bus submersion states. In addition, detection performance under low-light conditions remains an area that warrants further investigation.

(a) Detection outcomes obtained using YOLOv8n

(b) Detection outcomes obtained using YOLOv8s

(c) Detection outcomes obtained using YOLOv8m

(d) Detection outcomes obtained using YOLOv8l

Fig. 12. Comparison of YOLOv8 detection results in high flood risk scene with blurring and corruption (pre-augmentation): (a) Detection outcomes obtained using YOLOv8n; (b) Detection outcomes obtained using YOLOv8s; (c) Detection outcomes obtained using YOLOv8m; (d) Detection outcomes obtained using YOLOv8l.

3.3 Experimental results compared with YOLOv5

3.3.1 Analysis of training experiment results

Fig. 13 displays the precision-recall curves from the training results. A comparison reveals that YOLOv8s outperforms YOLOv5s on both the original and augmented datasets, indicating that YOLOv8s achieves higher detection accuracy in image recognition tasks. On the original dataset, YOLOv5s attains an mAP50 of 0.555, while YOLOv8s reaches 0.662, reflecting a performance gap of 19.3%. After data augmentation, although the performance gap between YOLOv5s and YOLOv8s narrows, YOLOv8s continues to lead. Additionally, results from the two training experiments with YOLOv5 indicate that data augmentation has a substantial impact on enhancing the training effectiveness of YOLO models
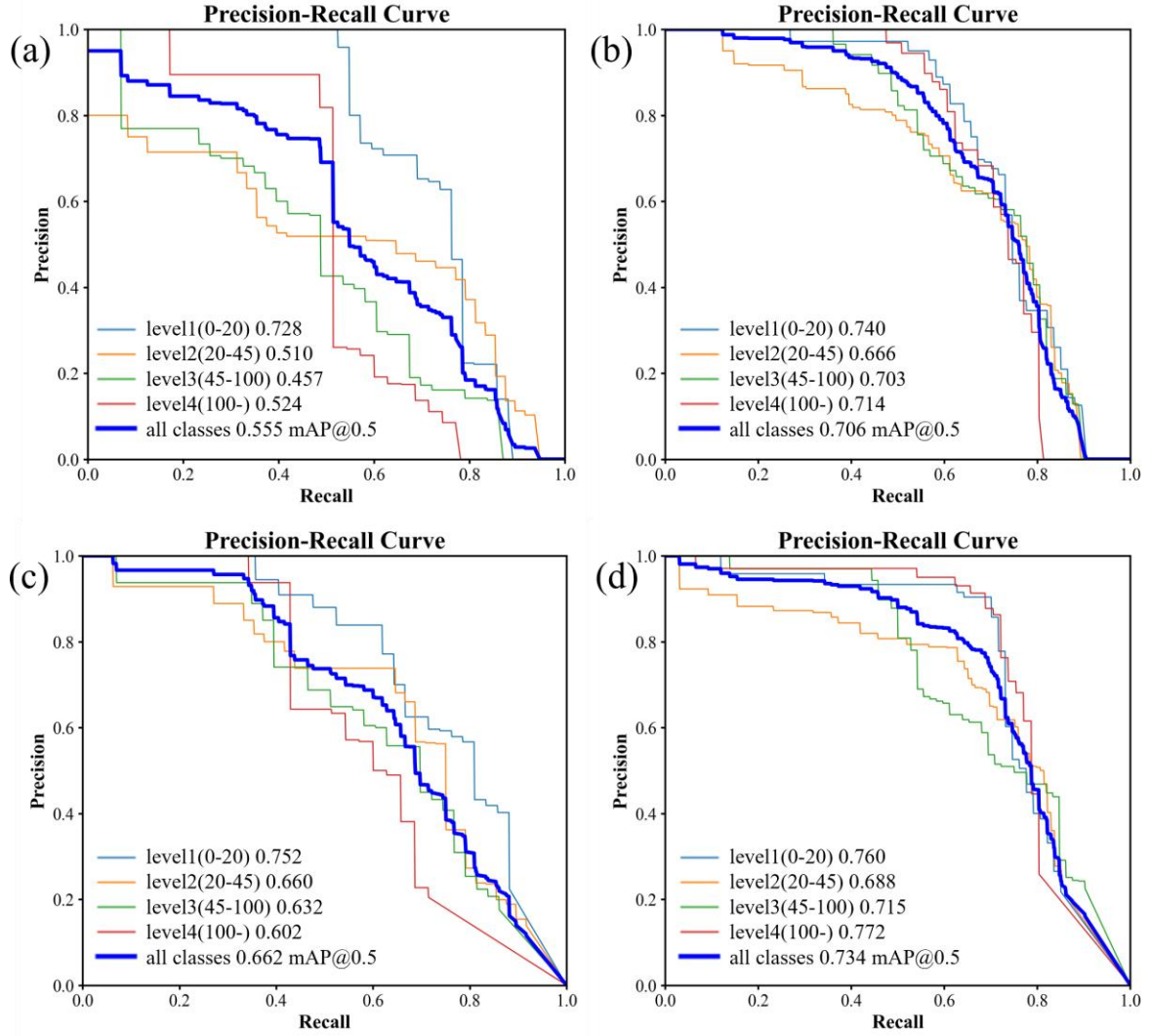
432 **Fig. 13.** Precision-recall curves from the training results: (a) YOLOv5s validation results on original dataset;
433 (b) YOLOv5s validation results on augmented dataset; (c) YOLOv8s validation results on original dataset;
434 (d) YOLOv8s validation results on augmented dataset.

435 **3.3.2 Analysis of scene prediction experiment results**

436   This section evaluates the stability and effectiveness of YOLOv5s and YOLOv8s under challenging

437 conditions by testing their performance in two complex urban scenes. Fig. 14 and Fig. 15 illustrate the

438 detection results of YOLOv5s and YOLOv8s in low and high flood risk scenes, respectively. In the low-risk

439 scene, YOLOv5s accurately identifies the bus and correctly predicts its submersion status, similar to

440 YOLOv8s; however, the confidence level of YOLOv5s, even after data augmentation, shows limited

441 improvement. YOLOv8s, on the other hand, demonstrates higher detection confidence and accuracy

442 following data augmentation. In the high-risk scene, characterized by blurred or partially degraded images,

443 YOLOv5s performs notably well. YOLOv5s detects targets that YOLOv8s fails to recognize, likely due to

444 its capacity for handling noisy data. This difference in performance under extreme conditions suggests that

445 the network structure of YOLOv5s may enhance detection in low-quality images, offering insights for

446 potential optimizations in YOLOv8s.

(a) YOLOv5s detection results on original dataset (b) YOLOv5s detection results on augmented dataset

(c) YOLOv8s detection results on original dataset (d) YOLOv8s detection results on augmented dataset

447
448 **Fig. 14.** Comparison of YOLO detection results in low flood risk scene with multiple vehicles present: (a)
449 YOLOv5s detection results on original dataset; (b) YOLOv5s detection results on augmented dataset; (c)
450 YOLOv8s detection results on original dataset; (d) YOLOv8s detection results on augmented dataset.
451

(a) YOLOv5s detection results on original dataset   (b) YOLOv5s detection results on augmented dataset

(c) YOLOv8s detection results on original dataset   (d) YOLOv8s detection results on augmented dataset

Fig. 15. Comparison of YOLO detection results in high flood risk scene with blurring and corruption: (a) YOLOv5s detection results on original dataset; (b) YOLOv5s detection results on augmented dataset; (c) YOLOv8s detection results on original dataset; (d) YOLOv8s detection results on augmented dataset.

4. Discussion

4.1 Impact of dataset size and diversity

The size and diversity of the training dataset play a critical role in determining the performance of YOLOv8 models. Models trained with the augmented dataset achieved substantial improvements, with mAP50 and mAP50-95 on the validation set increasing by over 10% and 20% (Table 3), across all YOLOv8 configurations. This improvement can be credited to the enhanced learning and generalization abilities of models. The increased number and diversity of training samples not only enable a more comprehensive understanding of the key features of detection targets but also allow for a broader representation of annotated instances, enhancing the model's ability to learn. Such exposure to varied input scenarios equips YOLOv8 with enhanced generalization, leading to better results in the validation stage.

Moreover, this benefit extends beyond training to inference capabilities. Under challenging conditions such as low illumination, motion blur, and partial occlusion, models trained on the augmented dataset exhibited greater robustness, reflected in higher detection confidence. Dataset diversity is therefore key to improving training performance and significantly enhancing inference in complex real-world environments.

470   The impact of dataset size and diversity varies across different YOLOv8 configurations. YOLOv8n,

471   with the smallest number of parameters, is particularly responsive to changes in training sample volume,

472   showing the most notable improvement in mAP when trained on the augmented dataset. In contrast,

473   YOLOv8s, which already performed well on the original dataset, shows the smallest relative gain.

474   Nevertheless, it consistently delivers the best results across multiple experiments.

475   **4.2 Recommended configurations for YOLOv8**

476   Based on the comprehensive performance of different YOLOv8 configurations during training and in

477   complex scenes, this study recommends prioritizing the YOLOv8s model for urban flood detection using

478   bus imagery. Although the YOLOv8l model theoretically offers higher network complexity and parameter

479   count, which should enable more granular feature extraction, its performance improvements in this

480   experiment were not significant. In contrast, the YOLOv8s model demonstrated superior results across

481   multiple performance metrics and achieved an effective balance between model accuracy, training time, and

482   computational resource requirements. Therefore, in environments with limited resources and high

483   computational costs, YOLOv8s has proven to be the most advantageous choice.

484   When computational resources and dataset availability are ample, YOLOv8m or YOLOv8l should be

485   considered as priority options. As dataset size expands and more computational resources become available,

486   the performance potential of YOLOv8m and YOLOv8l models may be more fully realized. With larger

487   datasets, the deeper network structures and advanced feature extraction capabilities of YOLOv8m and

488   YOLOv8l can better capture critical features and details of the targets, resulting in higher accuracy and

489   stability in object detection.

490   **4.3 Advantages and disadvantages**

491   Crowdsourced images from social media have emerged as a high-value data source for acquiring flood

492   information (Huang et al., 2020). The YOLO object detection model requires annotated images as input for

493   training, and such annotation can be performed by non-experts, making the method highly scalable. Buses,

494   as structurally standardized and dimensionally stable vehicles, provide reliable and scalable reference objects

495   for flood status identification. Moreover, buses typically operate in traffic-intensive or critical urban areas,

496   where water-related safety concerns directly impact the stability of the public transportation system. The bus

497   submergence detection technique adopted in this study significantly enhances the precision of urban flood

498 risk assessment, offering a more scientific basis for future flood monitoring and emergency response in cities.

499 Compared with existing studies, the method proposed in this paper demonstrates distinct advantages in

500 terms of reference object selection and object detection algorithms. The present study can be compared with

501 these approaches as follows: (Jiang et al., 2020), (Bhola et al., 2018) and (Alizadeh Kharazi and Behzadan,

502 2021) respectively utilized traffic cones and guardrails, bridge structures, and sign poles as reference

503 indicators. Although these objects offer advantages such as fixed structure and known physical dimensions,

504 their applicability is often confined to specific locations with fixed viewing angles and clearly visible

505 reference targets, and they are usually deployed only in limited areas. In contrast, this study adopts buses as

506 reference objects. Given their extensive operating routes and easily recognizable structural features, the

507 proposed method enables flood perception across broader urban road networks, thereby exhibiting enhanced

508 spatiotemporal adaptability.

509 (Huang et al., 2020) and (Park et al., 2021) applied the Mask R-CNN model to detect vehicle tires or

510 body structures to support flood level estimation. While their methods achieve high prediction accuracy,

511 Mask R-CNN is a two-stage detection framework with a complex architecture and relatively slow inference

512 speed. Additionally, it is highly sensitive to image quality and susceptible to errors under occlusion, water

513 splashes, or reflection interference—conditions common in real-world flood scenarios—which limits its

514 real-time applicability and environmental robustness (Huang et al., 2020). By contrast, the YOLOv8 model

515 adopted in this study is a single-stage, end-to-end detection framework. It demonstrates superior robustness

516 and detection speed under complex scene conditions and can stably identify reference targets, reducing false

517 detection rates. Its lightweight architecture also facilitates deployment on edge devices, making it suitable

518 for practical engineering applications.

519 (Wan et al., 2024) employed YOLOv8 to classify flood submergence levels of cars and achieved the

520 highest mAP50 of 0.707, demonstrating satisfactory detection accuracy. In their complex scenario testing,

521 sedans could be correctly identified, whereas pickup trucks failed to be recognized. This observation indicates

522 that the diversity of vehicle features may affect the model's generalization capability. In comparison, the

523 structural consistency and height stability of buses help reduce the impact of target variability on model

524 performance. Moreover, the best-performing model in this study achieved a mAP50 of 0.734, demonstrating

525 superior detection accuracy.

526 This study demonstrates that floodwater levels in urban areas can be effectively identified by detecting

527   the submergence status of buses using the YOLOv8 model. The proposed method has been validated in

528   terms of feasibility and practical potential. However, further research is warranted to enhance the model's

529   adaptability and applicability. On the one hand, the current dataset remains limited in scale, with insufficient

530   images under nighttime or low-light conditions, which constrains the model's performance under such

531   scenarios. Future work may incorporate illumination-guided transformers or light-aware attention

532   mechanisms to improve model robustness under challenging lighting environments. Simultaneously,

533   expanding the data acquisition scope and incorporating more diverse scenes will be critical for improving

534   detection accuracy. On the other hand, the current detection framework does not support quantitative

535   estimation of floodwater depth. Future research could explore regression-based modules that leverage the

536   actual height of buses and the geometric relationships within images to develop numerically interpretable

537   flood level estimators, thereby providing more actionable support for urban emergency response and flood

538   risk management.

539   **5. Conclusions**

540   This study proposes an urban flood detection method based on the YOLOv8 deep learning model, which

541   accurately assesses flood risk levels by identifying the submersion state of buses. A dataset of 1,008 images

542   depicting submerged buses was collected from online platforms and expanded to 2,184 images using data

543   augmentation strategies. Subsequently, the submersion states of buses were annotated into four levels for

544   training the object detection model. Finally, the performance of various YOLOv8 models was compared

545   through data augmentation and complex scene validation experiments, resulting in the following

546   experimental insights:

547   1)   The highest detection accuracy for flood risk levels is achieved by YOLOv8s. Although YOLOv8m

548   and YOLOv8l demonstrated comparable overall performance, they required significantly greater

549   computational resources and training time.

550   2)   Compared with commonly used reference objects in existing studies, buses offer advantages such as

551   structural standardization, consistent height, and wide spatial coverage, making them more suitable for

552   flood identification at the urban scale.

553   3)   This study offers configuration recommendations for YOLOv8 models tailored to urban flood

554   detection based on the submersion state of buses.

555   This study supplements and extends existing research on flood detection by validating the feasibility

556   and effectiveness of using buses as reference objects for the identification of urban flood risk levels. This

557   study explores the application potential of bus submersion state detection within the YOLOv8 framework.

558   This approach broadens the technical pathways for urban flood monitoring and provides crucial support for

559   flood emergency management within urban transportation systems, demonstrating practical value in the field

560   of disaster prevention and mitigation.

561   This study primarily relies on social media image recognition to determine flood risk levels. However,

562   the model still lacks robustness in certain complex scenarios, such as under extreme lighting conditions.

563   Additionally, the model currently lacks the capability to quantitatively measure flood depth, which is critical

564   for precise flood risk assessment. Future research will concentrate on devising methods for quantitative flood

565   depth estimation using bus submersion states and creating noise-resistant model architectures to improve the

566   model's applicability and precision.

567   **Data availability:**

568   Data will be made available on request.

569   **Declaration of competing interest**

570   The authors declare that they have no known competing financial interests or personal

571   relationships that could have appeared to influence the work reported in this paper.

572   **Computer Code Availability:**

573   The code in this study can be obtained from the Git repository:

574   https://github.com/ydkyly/dataset_and_result.git.

575   **Authorship Statement**

576   **Yanbin Qiu:** Writing – original draft, Validation, Software, Methodology, Investigation. **Xudong Zhou:**
577   Writing – review & editing, Validation. **Jiaquan Wan:** Writing – review & editing, Project administration,
578   Validation. **Tao Yang:** Writing – review & editing, Supervision. **Lvfei Zhang:** Formal analysis, Validation.
579   **Yuanzhuo Zhong:** Data curation, Validation. **Leqi Shen:** Data curation, Validation. **Xinwu Ji:** Validation.

580

References

Alizadeh Kharazi, B. and Behzadan, A. H.: Flood depth mapping in street photos with image processing and deep neural networks, Comput. Environ. Urban Syst., 88, 101628, https://doi.org/10.1016/j.compenvurbsys.2021.101628, 2021.

Baranowski, D. B., Flatau, M. K., Flatau, P. J., Karnawati, D., Barabasz, K., Labuz, M., Latos, B., Schmidt, J. M., Paski, J. A. I., and Marzuki: Social-media and newspaper reports reveal large-scale meteorological drivers of floods on Sumatra, Nat. Commun., 11, 2503, https://doi.org/10.1038/s41467-020-16171-2, 2020.

Betterle, A. and Salamon, P.: Water depth estimate and flood extent enhancement for satellite-based inundation maps, Nat. Hazards Earth Syst. Sci., 24, 2817–2836, https://doi.org/10.5194/nhess-24-2817-2024, 2024.

Bhola, P. K., Nair, B. B., Leandro, J., Rao, S. N., and Disse, M.: Flood inundation forecasts using validation data generated with the assistance of computer vision, J. Hydroinformatics, 21, 240–256, https://doi.org/10.2166/hydro.2018.044, 2018.

Chaudhary, P., D'Aronco, S., Leitão, J. P., Schindler, K., and Wegner, J. D.: Water level prediction from social media images with a multi-task ranking approach, ISPRS J. Photogramm. Remote Sens., 167, 252–262, https://doi.org/10.1016/j.isprsjprs.2020.07.003, 2020.

DeVries, B.: Rapid and robust monitoring of flood events using Sentinel-1 and Landsat data on the Google Earth Engine, Remote Sens. Environ., 2020.

Fohringer, J., Dransch, D., Kreibich, H., and Schröter, K.: Social media as an information source for rapid flood inundation mapping, Nat. Hazards Earth Syst. Sci., 15, 2725–2738, https://doi.org/10.5194/nhess-15-2725-2015, 2015.

Guan, Y., Zheng, F., Zhang, P., and Qin, C.: Spatial and temporal changes of meteorological disasters in China during 1950–2013, Nat. Hazards, 75, 2607–2623, https://doi.org/10.1007/s11069-014-1446-3, 2015.

Huang, J., Kang, J., Wang, H., Wang, Z., and Qiu, T.: A Novel Approach to Measuring Urban Waterlogging Depth from Images Based on Mask Region-Based Convolutional Neural Network, Sustainability, 12, 2149, https://doi.org/10.3390/su12052149, 2020.

Iqbal, U., Perez, P., Li, W., and Barthelemy, J.: How computer vision can facilitate flood management: A systematic review, Int. J. Disaster Risk Reduct., 53, 102030, https://doi.org/10.1016/j.ijdrr.2020.102030, 2021.

Jafari, N. H., Li, X., Chen, Q., Le, C.-Y., Betzer, L. P., and Liang, Y.: Real-time water level monitoring using live cameras and computer vision techniques, Comput. Geosci., 147, 104642, https://doi.org/10.1016/j.cageo.2020.104642, 2021.

Jiang, J., Liu, J., Cheng, C., Huang, J., and Xue, A.: Automatic Estimation of Urban Waterlogging Depths from Video Images Based on Ubiquitous Reference Objects, Remote Sens., 11, 587, https://doi.org/10.3390/rs11050587, 2019.

Jiang, J., Qin, C.-Z., Yu, J., Cheng, C., Liu, J., and Huang, J.: Obtaining Urban Waterlogging Depths from Video Images Using Synthetic Image Data, Remote Sens., 12, 1014, https://doi.org/10.3390/rs12061014, 2020.

Kankanamge, N., Yigitcanlar, T., Goonetilleke, A., and Kamruzzaman, Md.: Determining disaster severity through social media analysis: Testing the methodology with South East Queensland Flood tweets, Int. J. Disaster Risk Reduct., 42, 101360, https://doi.org/10.1016/j.ijdrr.2019.101360, 2020.

Kramer, M., Terheiden, K., and Wieprecht, S.: Safety criteria for the trafficability of inundated roads in urban floodings, Int. J. Disaster Risk Reduct., 17, 77–84, https://doi.org/10.1016/j.ijdrr.2016.04.003, 2016.

Kundu, S., Lakshmi, V., and Torres, R.: Flood Depth Estimation during Hurricane Harvey Using Sentinel-1 and UAVSAR Data, Remote Sens., 14, 1450, https://doi.org/10.3390/rs14061450, 2022.

Li, J., Cai, R., Tan, Y., Zhou, H., Sadick, A.-M., Shou, W., and Wang, X.: Automatic detection of actual water depth of urban floods from social media images, Measurement, 216, 112891, https://doi.org/10.1016/j.measurement.2023.112891, 2023.

Liang, J.: A local thresholding approach to flood water delineation using Sentinel-1 SAR imagery, ISPRS J. Photogramm. Remote Sens., 2020.

Nayak, S. and Zlatanova, S.: Remote sensing and GIS technologies for monitoring and prediction of disasters, Springer, Berlin London, 2008.

Park, S., Baek, F., Sohn, J., and Kim, H.: Computer Vision–Based Estimation of Flood Depth in Flooded-Vehicle Images, J. Comput. Civ. Eng., 35, 04020072, https://doi.org/10.1061/(ASCE)CP.1943-5487.0000956, 2021.

Paul, J. D., Buytaert, W., and Sah, N.: A Technical Evaluation of Lidar-Based Measurement of River Water Levels, Water Resour. Res., 56, e2019WR026810, https://doi.org/10.1029/2019WR026810, 2020.

Pregnolato, M., Ford, A., Wilkinson, S. M., and Dawson, R. J.: The impact of flooding on road transport: A depth-disruption function, Transp. Res. Part Transp. Environ., 55, 67–81, https://doi.org/10.1016/j.trd.2017.06.020, 2017.

Puliti, S. and Astrup, R.: Automatic detection of snow breakage at single tree level using YOLOv5 applied to UAV imagery, Int. J. Appl. Earth Obs. Geoinformation, 112, 102946, https://doi.org/10.1016/j.jag.2022.102946, 2022.

Qian, Y., Chakraborty, T. C., Li, J., Li, D., He, C., Sarangi, C., Chen, F., Yang, X., and Leung, L. R.: Urbanization Impact on Regional Climate and Extreme Weather: Current Understanding, Uncertainties, and Future Research Directions, Adv. Atmospheric Sci., 39, 819–860, https://doi.org/10.1007/s00376-021-1371-9, 2022.

Redmon, J., Divvala, S., Girshick, R., and Farhadi, A.: You Only Look Once: Unified, Real-Time Object Detection, in: 2016 IEEE Conference on Computer Vision and Pattern Recognition (CVPR), 2016 IEEE Conference on Computer Vision and Pattern Recognition (CVPR), Las Vegas, NV, USA, 779–788, https://doi.org/10.1109/CVPR.2016.91, 2016.

Rosser, J. F., Leibovici, D. G., and Jackson, M. J.: Rapid flood inundation mapping using social media, remote sensing and topographic data, Nat. Hazards, 87, 103–120, https://doi.org/10.1007/s11069-017-2755-0, 2017.

Smith, L., Liang, Q., James, P., and Lin, W.: Assessing the utility of social media as a data source for flood risk management using a real-time modelling framework, J. Flood Risk Manag., 10, 370–380, https://doi.org/10.1111/jfr3.12154, 2017.

Voulodimos, A., Doulamis, N., Doulamis, A., and Protopapadakis, E.: Deep Learning for Computer Vision: A Brief Review, Comput. Intell. Neurosci., 2018, 1–13, https://doi.org/10.1155/2018/7068349, 2018.

Wan, J., Qin, Y., Shen, Y., Yang, T., Yan, X., Zhang, S., Yang, G., Xue, F., and Wang, Q. J.: Automatic detection of urban flood level with YOLOv8 using flooded vehicle dataset, J. Hydrol., 639, 131625, https://doi.org/10.1016/j.jhydrol.2024.131625, 2024.

Yang, Z. and Wang, Q.: MINING METHOD OF TRAFFIC IMPACT AREAS OF RAINSTORM EVENT BASED ON SOCIAL MEDIA IN ZHENGZHOU CITY, Int. Arch. Photogramm. Remote Sens. Spat. Inf. Sci., XLVIII-3/W1-2022, 79–86, https://doi.org/10.5194/isprs-archives-XLVIII-3-W1-2022-79-2022, 2022.

666 Zhong, P., Liu, Y., Zheng, H., and Zhao, J.: Detection of Urban Flood Inundation from Traffic Images Using
667 Deep Learning Methods, Water Resour. Manag., 38, 287–301, https://doi.org/10.1007/s11269-023-03669-
668 9, 2024.

669